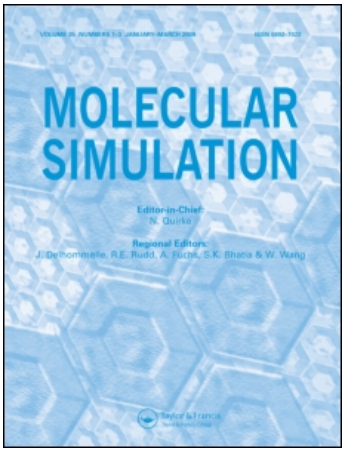

Molecular Simulation
Publication details, including instructions for authors and subscription information:
http://www.informaworld.com/smpp/title~content=t713644482

Vapour-Liquid Equilibria of Dipolar Two-Centre Lennard-Jones Fluids from a Physically Based Equation of State and Computer Simulations

Martin Lísal[a]; Karel Aim[a]; Johann Fischer[b]
[a] E. Hála Laboratory of Thermodynamics, Institute of Chemical Process Fundamentals, Academy of Sciences, Prague, Czech Republic [b] Institut für Land-, Umwelt- und Energietechnik, Universität für Bodenkultur, Wien, Austria

To cite this Article Lísal, Martin , Aim, Karel and Fischer, Johann(2000) 'Vapour-Liquid Equilibria of Dipolar Two-Centre Lennard-Jones Fluids from a Physically Based Equation of State and Computer Simulations', Molecular Simulation, 23: 6, 363 — 388
To link to this Article: DOI: 10.1080/08927020008023009
URL: http://dx.doi.org/10.1080/08927020008023009

Molecular Simulation, 2000, Vol. 23, pp. 363–388
Reprints available directly from the publisher
Photocopying permitted by license only

VAPOUR–LIQUID EQUILIBRIA OF DIPOLAR TWO-CENTRE LENNARD-JONES FLUIDS FROM A PHYSICALLY BASED EQUATION OF STATE AND COMPUTER SIMULATIONS

MARTIN LÍSAL[a,*], KAREL AIM[a] and JOHANN FISCHER[b]

[a]*E. Hála Laboratory of Thermodynamics, Institute of Chemical Process Fundamentals, Academy of Sciences, 165 02 Prague 6, Czech Republic;*
[b]*Institut für Land-, Umwelt- und Energietechnik, Universität für Bodenkultur, A-1190 Wien, Austria*

(Received October 1999; accepted October 1999)

The paper is concerned with the model fluid consisting of two-centre Lennard-Jones molecules with embedded axial dipole moment (2CLJD), particularly with its vapour–liquid phase equilibrium behaviour as calculated from different molecular simulation methods and from an analytical equation of state. The focus of the present study is the parameter region of large elongations (L in the range from 0.505 to 1.0) and large dipole moments (μ^{*2} in the range from 9 to 12) of the 2CLJD fluid. In order to assess the performance of independent molecular simulation methods and to examine the validity of a physically based equation of state of the augmented van der Waals type within this parametric region, we have calculated the 2CLJD model fluid properties along the vapour–liquid coexistence locus by the Gibbs ensemble Monte Carlo method, Gibbs-Duhem integration technique looking at the effect of different starting state points, the NpT plus test particle method, and from the equation of state. Within the entire region examined, fairly good mutual agreement of the independent simulation methods is observed. The equation of state represents a good compromise between the results of different simulation methods at intermediate elongations but fails at large elongations. The extended base of pseudoexperimental data is prerequisite for further equation of state development.

Keywords: Dipolar two-centre Lennard-Jones fluid; equation of state; intermolecular interactions; molecular simulation; vapour–liquid equilibria

*Corresponding author.

1. INTRODUCTION

The simplest molecular models of dipolar fluids with nonspherical molecules are model fluids consisting of two-centre Lennard-Jones molecules with an axial dipole moment (2CLJD). In a series of papers [1–4], a physically based equation of state (EOS) was developed for the 2CLJD fluids. The EOS is written in the form of a generalized augmented van der Waals equation for the Helmholtz energy, $F = F_H + F_A + F_D$, where F_H accounts for the hard-body interaction, F_A for the attractive dispersion forces and F_D for the dipolar contribution.

The hard-body term F_H was represented by the expression due to Boublík and Nezbeda [5] based on the scaled particle theory with temperature dependence of the packing fraction resulting from the so called hybrid Barker-Henderson perturbation theory [6].

The attractive contribution F_A was obtained by using extensive molecular dynamics (MD) simulations on 2CLJ fluids with molecular elongations L ranging from 0 to 0.67 [3]. Second virial coefficients and vapour–liquid equilibrium (VLE) data from the NpT plus test particle (NpT+TP) method were also included in the data base for the fit of the functional form for F_A [3]. Comparison of pressure–volume–temperature (PVT) and VLE data obtained from the EOS with independent simulation data for the Lennard-Jones fluid [7] and the 2CLJ fluid with $L = 0.505$ [8] shows that the EOS represents simulation data mostly within their statistical uncertainties.

The dipolar contribution F_D was derived *via* the λ-coupling technique [2] on the basis of extensive MD simulations on 2CLJD fluids with $L = 0.505$ and values of the square of reduced dipole moments μ^{*2} reaching up to 12 [9]. Comparison of VLE data from the EOS with independent Gibbs ensemble Monte Carlo (GEMC) and NpT + TP data for Stockmayer fluid shows good to excellent agreement [10, 11]. The contribution F_D was originally constructed so as to be independent of the molecular elongation L. Investigations of Müller *et al.* [12] showed that F_D is weakly dependent on L at large dipole moments.

A question then arises on how accurately the EOS is able to describe VLE of 2CLJD fluids with large dipole moments and molecular elongations L greater than 0.67. Answer to this question is very important because at moderate elongations and dipolarity good to excellent predictions of thermodynamic and VLE data of both (i) real fluids (if potential parameters are derived from few points on VLE curve only [4, 13–15]) and (ii) model and real mixtures (if appropriate mixing rules are used [10, 16]) can be expected by using the EOS for the 2CLJD fluids.

Another important issue is the accuracy and performance of the direct computer simulation methods used to calculate VLE for the 2CLJD fluids. In our so far carried out studies [17, 18] we have detected certain discrepancies depending on L, μ^{*2} and on the starting point of the Gibbs-Duhem integration.

The purpose of this paper is thus twofold: (i) to examine thoroughly the EOS for 2CLJD fluid over wide ranges of L (0.505 to 1.0) and μ^{*2} (up to 12) on the basis of VLE data obtained by the direct computer simulation methods, namely by the NpT + TP method [19], Gibbs-Duhem integration (GDI) [20] and GEMC [21] and (ii) to assess and discuss systematically the performance of the above mentioned direct simulation methods for VLE calculations in the case of the 2CLJD fluids, particularly over the considered parameteric region.

2. INTERMOLECULAR POTENTIAL

The intermolecular potential for the 2CLJD fluid, $u_{2\mathrm{CLJD}}$, is

$$u_{2\mathrm{CLJD}}(r,\omega_i,\omega_j) = u_{2\mathrm{CLJ}}(r,\omega_i,\omega_j) + u_D(r,\omega_i,\omega_j) \tag{1}$$

where r is the distance between centres of mass of molecule j and molecule i, and ω_i and ω_j are the orientations of molecules. The 2CLJ interaction, $u_{2\mathrm{CLJ}}$, is defined as

$$u_{2\mathrm{CLJ}}(r,\omega_i,\omega_j) = \sum_{a=1}^{2}\sum_{b=1}^{2} 4\varepsilon\left[\left(\frac{\sigma}{r_{ab}}\right)^{12} - \left(\frac{\sigma}{r_{ab}}\right)^{6}\right] \tag{2}$$

In Eq. (2), r_{ab} is the distance between atom a of molecule i and atom b of molecule j, and ε and σ are the Lennard-Jones energy and size parameters, respectively. The interaction between two axial dipole moments and $\boldsymbol{\mu}_i$ and $\boldsymbol{\mu}_j$, u_D, is given as

$$u_D(r,\omega_i,\omega_j) = -\frac{1}{4\pi\varepsilon_0}\boldsymbol{\mu}_i\mathbf{T}(\mathbf{r})\boldsymbol{\mu}_j \tag{3}$$

where $\mathbf{r} = \mathbf{r}_j - \mathbf{r}_i$ is the distance vector between centres of mass of molecules j and i. Dipole–dipole tensor $\mathbf{T}(\mathbf{r})$ is given by

$$T_{ab} = \frac{3r_a r_b}{r^5} - \frac{\delta_{ab}}{r^3} \tag{4}$$

with Kronecker's symbol δ_{ab}.

In the following, we use reduced quantities as follows: molecular elongation $L = l/\sigma$, l is the bond length; time step $\Delta t^* = \Delta t/(\sigma\sqrt{(m/\varepsilon)})$, m is the mass of the 2CLJD molecule; temperature $T^* = k_B T/\varepsilon$, k_B is the Boltzmann constant; number density $\rho^* = \rho\sigma^3$; pressure $p^* = p\sigma^3/\varepsilon$; second virial coefficient $B^* = B/\sigma^3$; potential energy $u^* = U/N\varepsilon$; enthalpy $h^* = H/N\varepsilon$; Helmholtz energy $f^* = F/N\varepsilon$, and square of dipole moment $\mu^{*2} = \mu^2/(4\pi\varepsilon_0\varepsilon\sigma^3)$, ε_0 is the permittivity of free space.

3. DETERMINATION OF VAPOUR–LIQUID EQUILIBRIA

In this section we briefly describe the methods used to calculate the VLE coexistence locus in the present study, namely the NpT+TP and GDI methods. Further details on simulations are given in Section 4. Principles of the GEMC method [21] are well known and we will not repeat them here. Moreover, the methods to calculate VLE from an EOS are also shortly reviewed.

3.1. Equation of State

Using the physically based EOS for the 2CLJD fluids [4], $F = F_H + F_A + F_D$, VLE can be determined from equalities of temperature, pressure and chemical potential in the vapour and liquid phases. From the EOS (see Appendix for detailed form), pressure p^* and chemical potential μ^* are obtained using the standard thermodynamic relationships

$$p^* = \rho^* T^* + \rho^{*2} \frac{\partial f^*}{\partial \rho^*} \tag{5}$$

$$\mu^* = f^* - T^* + T^* \ln \rho^* + \frac{p^*}{\rho^*} \tag{6}$$

An alternative (and equivalent) way of determining the VLE is to apply the Maxwell equal-area rule

$$p_\sigma^* \left(\frac{1}{\rho_v^*} - \frac{1}{\rho_l^*} \right) = - \int_{\rho_v^*}^{\rho_l^*} p^* \frac{d\rho^*}{\rho^{*2}} \tag{7}$$

In Eq. (7), p_σ^* is the saturated pressure, ρ_v^* is the saturated-vapour density, and ρ_l^* is the saturated-liquid density. For thermodynamically consistent EOS, both ways of determination of VLE are mathematically identical. In our numerical evaluation, both routes gave also identical results.

3.2. NpT Plus Test Particle Method

The basic idea of the NpT+TP method is to construct at a given temperature the liquid and vapour branches in the chemical potential *vs.* pressure plane and, subsequently, to find the point of intersection of these two branches [19]. The chemical potential is evaluated by means of the Widom's insertion method [22]. Hence, the NpT+TP method like the GEMC runs into problems in the region of high densities. At lower temperatures, the saturated-vapour densities are rather low and hence the vapour branch in the chemical potential *vs.* pressure plane can be precisely determined using a convenient simple EOS, *e.g.*, the truncated virial EOS.

3.3. Gibbs-Duhem Integration

The Gibbs-Duhem integration method [20] is based on numerical solution of the Clapeyron equation that can be written as follows

$$\left(\frac{d\ln p^*}{d(1/T^*)}\right)_\sigma = -\frac{T^*}{p^*}\frac{h_v^* - h_l^*}{1/\rho_v^* - 1/\rho_l^*} \tag{8}$$

In Eq. (8), h_v^* and h_l^* are the vapour and liquid enthalpy, respectively. Clapeyron equation is the first-order nonlinear differential equation expressing the pressure as a function of temperature along the VLE coexistence region. Given an initial condition, *i.e.*, the pressure, temperature, and saturated densities and enthalpies at one coexistence point, Eq. (8) can be solved numerically by a predictor-corrector method [8, 20]. The quantities needed to evaluate the right-hand side of the Clapeyron equation are obtained from simultaneous (but independent) NPT MD simulations of the liquid and vapour phases. It should be noted that the GDI in contrast to both the NpT+TP and GEMC methods does not rely on particle insertion and so it can be used for determination of phase equilibria at high densities.

As in the NpT+TP case, the GDI can be modified to incorporate thermodynamic description of the vapour phase at lower temperatures [8], allowing so to skip the simulations of the vapour phase. We implemented the simple truncated virial equation of state

$$\frac{p^*}{\rho^* T^*} = 1 + B^* \rho^* \tag{9}$$

wherein the second virial coefficient B^* was calculated by the non-product algorithm [23]. The calculated values of B^* were represented by the equation

employed in Ref. [24]

$$B^*(T^*) = a_1\left\{1 - a_2\left[\exp\left(\frac{a_3}{T^*}\right) - 1\right]\right\} \tag{10}$$

The vapour density ρ_v^* was obtained from the simple truncated virial EOS as

$$\rho_v^* = \frac{\sqrt{4B^* p_\sigma^*/T^* + 1} - 1}{2B^*} \tag{11}$$

and the difference in enthalpies $h_v^* - h_l^*$ was expressed according to [25] by

$$h_v^* - h_l^* = -u_l^* + p^*\left(\frac{1}{\rho_v^*} - \frac{1}{\rho_l^*}\right) + \rho_v^* T^*\left(T^*\frac{dB^*}{dT^*} - B^*\right) \tag{12}$$

In Eq. (12), u_l^* is the potential energy of the liquid.

As already mentioned the use of the GDI method requires knowledge of one starting coexistence point that must be determined by an independent method. We initialized GDI runs from coexistence points determined by (i) Maxwell constructions at moderate and high temperatures, and (ii) GEMC at a high temperature in order to assess and discuss influence of the starting coexistence point on the accuracy of the GDI method. For the Maxwell constructions, we carried out NVT MD simulations for typically 30 densities covering the range of vapour–liquid coexistence. Results of NVT MD simulations were correlated by equation

$$\frac{p^*}{\rho^* T^*} = 1 + a_1\rho^* + a_2\rho^{*2} + a_3\rho^{*3} + a_4\rho^{*4} + a_5\rho^{*5} + a_6\rho^{*10} \tag{13}$$

Equation (13) is based on the expression for compressibility factor derived by Hansen from the perturbation theory [26] and represents simulations data within their statistical uncertainties.

4. SIMULATION DETAILS

4.1. NPT Molecular Dynamics Simulation

For the NpT + TP method as well as for the GDI method we carried out the NPT MD simulations by using the Andersen algorithm [22]. The

temperature was kept constant by the isokinetic scaling of translational and angular velocities after every timestep. The equations of the translational motion were solved by the Gear predictor – corrector algorithm of the fifth order. Rotational motion was treated by the method of quaternions and it was solved by the Gear predictor – corrector algorithm of the fourth order [22]. The minimum image convention, periodic boundary conditions and cut-off radius equal to the half-box length were used. The 2CLJ long-range corrections of the internal energy and pressure were included assuming that radial distribution functions are unity beyond the cut-off radius [22]. The dipolar long-range corrections of internal energy and pressure were treated by the reaction field method with dielectric constant ε_{RF} set to infinity [9]. For the integration, timestep $\Delta t^* = 0.0015$ was chosen. The membrane mass M^* was set to $5 \cdot 10^{-4}$ for the liquid and $1 \cdot 10^{-6}$ for the vapour. All simulation runs were performed with 256 molecules. At each temperature, equilibrium period took 5000 timesteps, and subsequently typically 50000 timesteps were used to collect the ensemble averages. For the NpT + TP method the chemical potential was calculated by using Widom's insertion method; 256 test particles were inserted after every timestep. Further simulation details about the GDI method can be found in [17, 18] and about the NpT + TP method in [4, 27].

4.2. Gibbs Ensemble Monte Carlo Method

GEMC simulations [21] were organized in cycles. Each cycle consisted of three steps: n_d translation and rotational moves, one volume move and n_i particle transfers. The three types of moves were selected at random with fixed probabilities chosen so that the appropriate ratios of each type of move were obtained. The ratio of steps 'particle transfer : attempted displacement : volume change' in the GEMC cycle was set to 1000 : 100 : 1 [21]. The GEMC simulations started with 256 molecules on an fcc lattice in each cubic box. After equilibration period, further $(4-6) \times 10^5$ cycles were carried out to accumulate ensemble averages. Length of equilibration period was determined from convergence profiles [28] of the coexisting densities and internal energies and included about $(1-2) \times 10^5$ cycles. The final configurations were then used as the starting point for subsequent GEMC simulations. The acceptance ratios of displacement and volume moves were adjusted to about 30%. Number of successful particle interchanges was (0.5–5)% per cycle with lower values at lower temperatures.

5. RESULTS AND DISCUSSION

In order to assess in detail the performance of the direct computer simulation methods for the calculation of VLE, we have simulated VLE data of the 2CLJD fluid for elongation $L = 0.505$ and values of the square of reduced dipole moment $\mu^{*2} = 9$ and 12 for temperature range from $T^* = 2.45$ to 3.1 and from $T^* = 2.4$ to 3.2, respectively. We used the GEMC method, the NpT+TP method (only for the case with $\mu^{*2} = 9$), and the GDI method in three versions differing in the choice of the starting state points and their determination: (i) in the first type of run (in the following designated as GDI1), the GDI was started from the Maxwell construction produced by NVT MD simulation at a moderate temperature; (ii) in the second type of run (designated hereafter as GDI2), the GDI was started from an analogous Maxwell construction at a high temperature; and (iii) in the third type of run (in the following designated as GDI3), the GDI was initiated from a VLE coexistence point generated by the GEMC at a high temperature. The vapour phase was represented by the simple truncated virial EOS in the GDI3 run to avoid the ineffective sampling of a low-density vapour system. In addition, VLE data over the considered regions of conditions were also determined from the physically based EOS described in the Appendix. The simulation results along with the corresponding data obtained from the EOS and comparisons are fully documented in Tables I and II and their illustrative subsets are visualized in Figures 1 to 4.

Further, in order to examine primarily the accuracy and extrapolation power of the physically based EOS in the region of large molecular elongations and high dipole moments we have also directly simulated VLE for the 2CLJD fluid for all the combinations of elongations $L = 0.8$ and 1.0 and dipole moments $\mu^* = 9$ and 12. In these cases, we used the GEMC method at three temperatures covering the entire studied range and the GDI3 version starting at a moderately high temperature. The obtained VLE simulation data along with the corresponding values calculated from the EOS are listed in Tables III to VI and selected views of their comparisons are shown in Figures 5 and 6.

5.1. Performance of Direct Simulation Methods and Physically Based Equation of State

As it can be seen from Table I and Figures 1 and 2 (wherein for practical reasons the data calculated from the physically based EOS are taken as a reference base line) the performance of all direct simulation methods

TABLE I Comparison of vapour–liquid equilibrium data for the 2CLJD fluid with $L = 0.505$ and $\mu^{*2} = 9$ obtained from the physically based equation of state, Eq. (14), and direct simulations. The simulation uncertainties are given in the last digits as subscripts. The percentagewise deviations of the simulation data from the equation of state are given in parentheses. EOS denotes data from the equation of state, GDI1 is the Gibbs-Duhem integration method starting from the Maxwell construction at $T^* = 2.7$, GDI2 is the Gibbs-Duhem integration method starting from the Maxwell construction at $T^* = 3.1$, GDI3 is the Gibbs-Duhem integration method starting from the Gibbs ensemble Monte Carlo coexistence point at $T^* = 3.1$ and using description of the vapour phase by the simple truncated virial equation of state, Eq. (11), at $T^* < 2.9$, NpT+TP is the NpT plus test particle method, and GEMC denotes the Gibbs ensemble Monte Carlo simulations. Vapour densities evaluated from the simple truncated virial equation of state, Eq. (11), at the vapour pressures are also added in parentheses

T^*	*EOS*	*GDI1*	*GDI2*	*GDI3*	*NpT+TP*	*GEMC*
Vapour pressures						
2.45	0.0145	$0.0149_{14}(-3.0\%)$	$0.0141_{17}(2.5\%)$	$0.0135_{16}(6.6\%)$	$0.0136_{9}(5.9\%)$	
2.5	0.0173	$0.0180_{25}(-4.3\%)$	$0.0171_{8}(0.9\%)$	$0.0162_{15}(6.1\%)$	$0.0152_{10}(11.9\%)$	$0.0171_{28}(0.9\%)$
2.6	0.0240	$0.0256_{15}(-6.6\%)$	$0.0244_{12}(-1.6\%)$	$0.0229_{14}(4.7\%)$	$0.0234_{13}(2.6\%)$	
2.7	0.0326	$0.0352(-7.9\%)$	$0.0338_{18}(-3.6\%)$	$0.0322_{20}(1.3\%)$	$0.0296_{18}(9.3\%)$	
2.8	0.0434	$0.0469_{24}(-8.2\%)$	$0.0454_{23}(4.7\%)$	$0.0450_{21}(-3.8\%)$	$0.0446_{30}(-2.9\%)$	$0.0414_{68}(4.5\%)$
2.9	0.0565	$0.0614_{24}(-8.7\%)$	$0.0593_{27}(-5.0\%)$	$0.0538_{24}(4.8\%)$	$0.0532_{34}(5.8\%)$	
3.0	0.0725	$0.0788_{18}(-8.7\%)$	$0.0760_{17}(-4.8\%)$	$0.0684_{20}(5.7\%)$	$0.0734_{26}(-1.2\%)$	
3.1	0.0917	$0.0997_{18}(-8.7\%)$	$0.0958(-4.5\%)$	$0.0861(6.1\%)$	$0.0914_{28}(0.3\%)$	$0.0861_{112}(6.1\%)$
Saturated liquid densities						
2.45	0.4878	$0.4878_{5}(0.0\%)$	$0.4876_{5}(0.0\%)$	$0.4891_{5}(-0.3\%)$	$0.4878_{6}(0.0\%)$	
2.5	0.4809	$0.4810_{5}(0.0\%)$	$0.4812_{6}(0.0\%)$	$0.4821_{5}(-0.2\%)$	$0.4793_{7}(0.4\%)$	$0.4850_{5}(-0.8\%)$
2.6	0.4666	$0.4654_{7}(0.3\%)$	$0.4673_{6}(-0.1\%)$	$0.4676_{6}(-0.2\%)$	$0.4664_{8}(0.1\%)$	
2.7	0.4515	$0.4543(-0.6\%)$	$0.4500_{7}(0.4\%)$	$0.4516_{8}(0.0\%)$	$0.4503_{9}(0.3\%)$	
2.8	0.4354	$0.4350_{10}(0.1\%)$	$0.4356_{11}(0.0\%)$	$0.4340_{10}(0.3\%)$	$0.4378_{9}(-0.5\%)$	$0.4376_{10}(-0.5\%)$
2.9	0.4179	$0.4189_{11}(-0.3\%)$	$0.4170_{8}(0.2\%)$	$0.4166_{10}(0.3\%)$	$0.4174_{12}(0.1\%)$	
3.0	0.3987	$0.3985_{9}(0.1\%)$	$0.3995_{12}(-0.2\%)$	$0.3971_{11}(0.4\%)$	$0.3966_{12}(0.5\%)$	
3.1	0.3770	$0.3796_{13}(-0.7\%)$	$0.3819(-1.3\%)$	$0.3758(0.3\%)$	$0.3781_{15}(-0.3\%)$	$0.3758_{18}(0.3\%)$

TABLE I (Continued)

T^*	*EOS*	*GDI*1	*GDI*2	*GDI*3	*NpT+TP*	*GEMC*
Saturated vapour densities						
2.45	0.0066	0.0079_{8}(−19.0%)	0.0077_{10}(−16.0%)	0.0060(9.6%)	0.0063_{5}(5.1%)	
	(0.0067)	(0.0069)	(0.0065)	(0.0060)	(0.0063)	
2.5	0.0079	0.0096_{17}(−21.9%)	0.0088_{7}(−11.7%)	0.0072(8.6%)	0.0069_{5}(12.4%)	0.0081_{16}(−2.9%)
	(0.0080)	(0.0084)	(0.0079)	(0.0072)	(0.0069)	(0.0079)
2.6	0.0109	0.0126_{13}(−15.4%)	0.0119_{10}(−9.0%)	0.0102(6.6%)	0.0108_{8}(1.0%)	
	(0.0111)	(0.0121)	(0.0114)	(0.0102)	(0.0108)	
2.7	0.0149	0.0157(−5.6%)	0.0161_{17}(−8.3%)	0.0145(2.5%)	0.0135_{11}(9.2%)	
	(0.0154)	(0.0172)	(0.0162)	(0.0145)	(0.0135)	
2.8	0.0200	0.0222_{22}(−11.0%)	0.0213_{20}(−6.5%)	0.0210(−5.2%)	0.0223_{25}(−11.5%)	0.0200_{43}(0.0%)
	(0.0207)	(0.0243)	(0.0229)	(0.0210)	(0.0223)	(0.0198)
2.9	0.0268	0.0284_{21}(−4.1%)	0.0270_{21}(−1.2%)	0.0251_{21}(5.9%)	0.0267_{31}(−0.1%)	
	(0.0301)	(0.0390)	(0.0340)	(0.0272)	(0.0267)	
3.0	0.0356	0.0373_{28}(−4.8%)	0.0351_{23}(−1.4%)	0.0342_{18}(3.9%)	0.0376_{18}(−5.6%)	
3.1	0.0478	0.0511_{80}(−6.9%)	0.0457(4.4%)	0.0482(−0.7%)	0.0488_{24}(−2.1%)	0.0482_{124}(−0.7%)

TABLE II Comparison of vapour–liquid equilibrium data for the 2CLJD fluid with $L = 0.505$ and $\mu^{*2} = 12$ obtained from the physically based equation of state, Eq. (14), and direct simulations. The simulation uncertainties are given in the last digits as subscripts. The percentagewise deviations of the simulation data from the equation of state are given in parentheses. EOS denotes data from the equation of state, GDI1 is the Gibbs-Duhem integration method starting from the Maxwell construction at $T^* = 2.8$, GDI2 is the Gibbs-Duhem integration method starting from the Maxwell construction at $T^* = 3.2$, GDI3 is the Gibbs-Duhem integration method starting from the Gibbs ensemble Monte Carlo coexistence point at $T^* = 3.2$ and using description of the vapour phase by the simple truncated virial equation of state, Eq. (11), at $T^* < 2.9$, and GEMC denotes the Gibbs ensemble Monte Carlo simulations. Vapour densities evaluated from the simple truncated virial equation of state, Eq. (11), at the vapour pressures are also added in parentheses

T^*	*EOS*	*GDI1*	*GDI2*	*GDI3*	*GEMC*
Vapour pressures					
2.4	0.0046	0.0037_4(18.7%)	0.0039_6(14.3%)	0.0043_5(5.5%)	0.0049_{11}(−7.7%)
2.5	0.0069	0.0056_7(18.6%)	0.0061_8(11.3%)	0.0065_7(5.5%)	
2.6	0.0101	0.0085_8(15.4%)	0.0091_7(9.5%)	0.0095_9(5.5%)	
2.7	0.0142	0.0123_8(13.4%)	0.0133_{12}(6.3%)	0.0137_{11}(3.5%)	0.0133_{33}(6.6%)
2.8	0.0197	0.0175(11.0%)	0.0191_{11}(2.8%)	0.0194_{13}(1.3%)	
2.9	0.0265	0.0239_{16}(9.8%)	0.0265_{21}(0.0%)	0.0253_{16}(4.6%)	
3.0	0.0351	0.0323_{27}(7.9%)	0.0360_{26}(−2.7%)	0.0334_{23}(4.8%)	
3.1	0.0456	0.0426_{26}(6.6%)	0.0476_{31}(−4.4%)	0.0414_{25}(9.2%)	
3.2	0.0584	0.0548_{32}(6.2%)	0.0617(−5.6%)	0.0532(8.8%)	0.0532_{91}(8.8%)
Saturated liquid densities					
2.4	0.5210	0.5199_5(0.2%)	0.5220_4(−0.2%)	0.5202_5(0.2%)	0.5331_6(−2.3%)
2.5	0.5093	0.5103_6(−0.2%)	0.5093_6(0.0%)	0.5097_6(−0.1%)	
2.6	0.4972	0.4974_6(−0.1%)	0.4977_5(−0.1%)	0.4984_5(−0.3%)	
2.7	0.4846	0.4851_7(−0.1%)	0.4845_5(0.0%)	0.4859_6(−0.3%)	0.4904_9(−1.2%)
2.8	0.4716	0.4741(−0.5%)	0.4713_6(0.1%)	0.4730_6(−0.3%)	
2.9	0.4579	0.4583_6(−0.1%)	0.4599_7(−0.4%)	0.4588_7(−0.2%)	
3.0	0.4436	0.4436_7(0.0%)	0.4463_7(−0.6%)	0.4443_8(−0.2%)	
3.1	0.4283	0.4302_{10}(−0.4%)	0.4274_{10}(0.2%)	0.4266_{15}(0.4%)	
3.2	0.4118	0.4135_{11}(−0.4%)	0.4156(−0.9%)	0.4120(0.0%)	0.4120_{14}(0.0%)
Saturated vapour densities					
2.4	0.0020	0.0018_2(10.9%)	0.0019_3(6.0%)	0.0018(10.9%)	0.0023_5(−13.8%)
	(0.0021)	(0.0016)	(0.0017)	(0.0018)	(0.0022)
2.5	0.0030	0.0027_4(9.7%)	0.0030_7(−0.4%)	0.0027(9.7%)	
	(0.0030)	(0.0024)	(0.0026)	(0.0027)	
2.6	0.0043	0.0043_5(−0.2%)	0.0045_{14}(−4.8%)	0.0040(6.8%)	
	(0.0044)	(0.0036)	(0.0039)	(0.0040)	
2.7	0.0060	0.0061_4(−1.7%)	0.0069_{13}(−15.0%)	0.0057(5.0%)	0.0058_{17}(3.3%)
	(0.0061)	(0.0052)	(0.0057)	(0.0057)	(0.0056)
2.8	0.0083	0.0073(11.6%)	0.0099_{14}(−19.8%)	0.0079(4.4%)	
	(0.0085)	(0.0074)	(0.0082)	(0.0079)	
2.9	0.0112	0.0117_{14}(−4.5%)	0.0129_{14}(−15.2%)	0.0112_{11}(0.2%)	
	(0.0117)	(0.0102)	(0.0117)	(0.0110)	
3.0	0.0149	0.0160_{22}(−7.3%)	0.0175_{25}(−17.4%)	0.0151_{19}(1.3%)	
	(0.0161)	(0.0142)	(0.0168)	(0.0149)	
3.1	0.0197	0.0191_{27}(3.0%)	0.0226_{23}(−14.7%)	0.0183_{16}(7.2%)	
	(0.0229)	(0.0200)	(0.0255)	(0.0190)	
3.2	0.0261	0.0249_{36}(4.6%)	0.0257(1.6%)	0.0252(3.4%)	0.0252_{60}(3.4%)

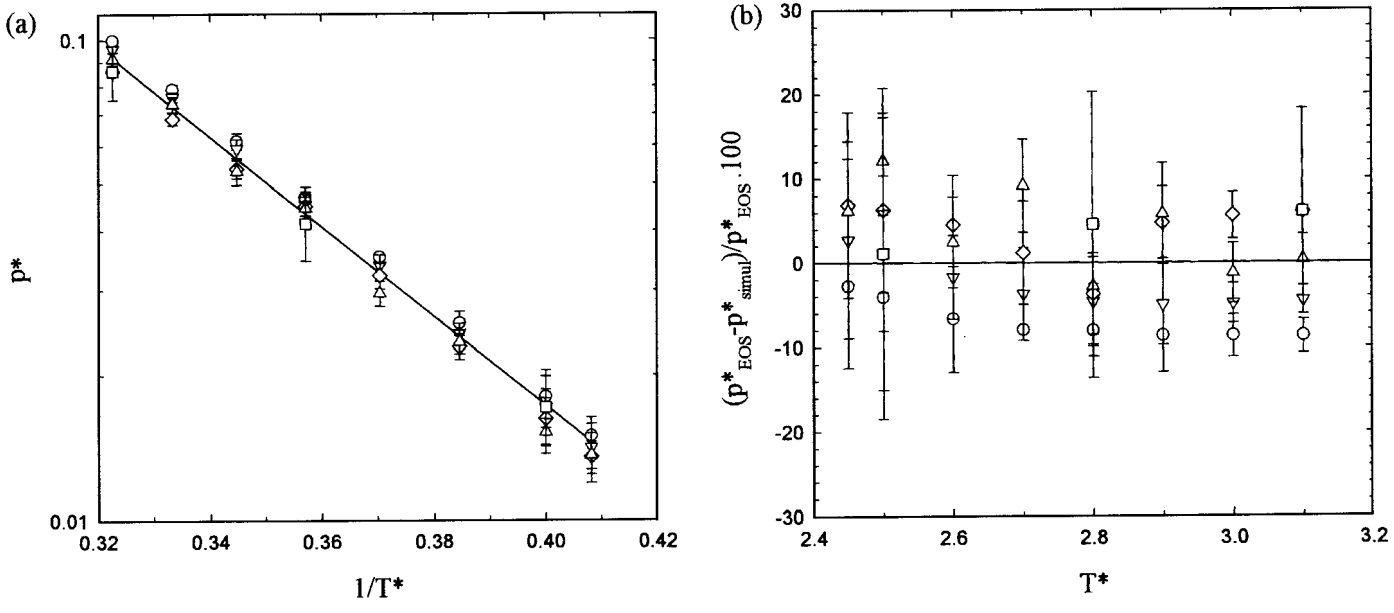

FIGURE 1 (a) Vapour pressure and (b) its relative deviations for 2CLJD fluid with $L = 0.505$ and $\mu^{*2} = 9$. (—, EOS; ○, GDI1; ▽, GDI2; ◇, GDI3; △, NpT+TP; □, GEMC; see Tab. I for explanation of acronyms).

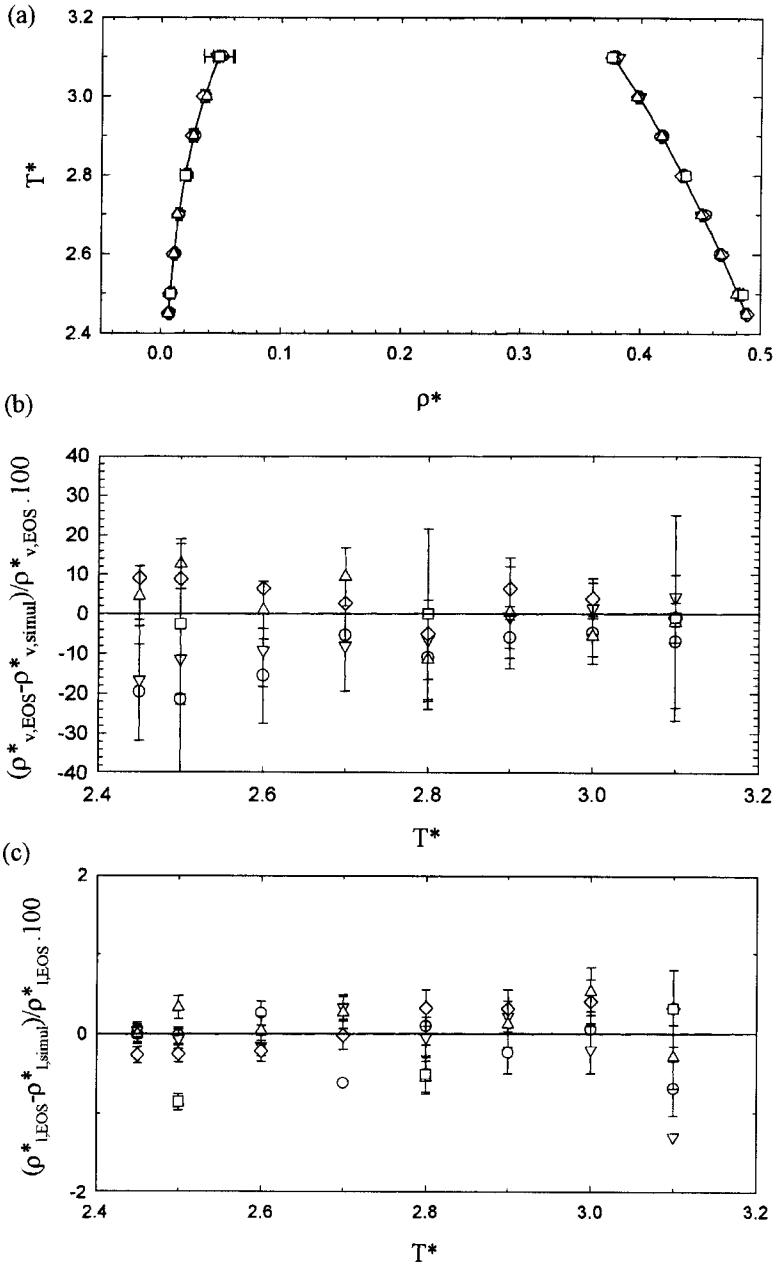

FIGURE 2 (a) Vapour–liquid coexistence envelope (b) relative deviations in saturated vapour density and (c) relative deviations in saturated liquid density for 2CLJD fluid with $L = 0.505$ and $\mu^{*2} = 9$. (—, EOS; ○, GDI1; ▽, GDI2; ◇, GDI3; △, NpT+TP; □, GEMC; see Tab. I for explanation of acronyms).

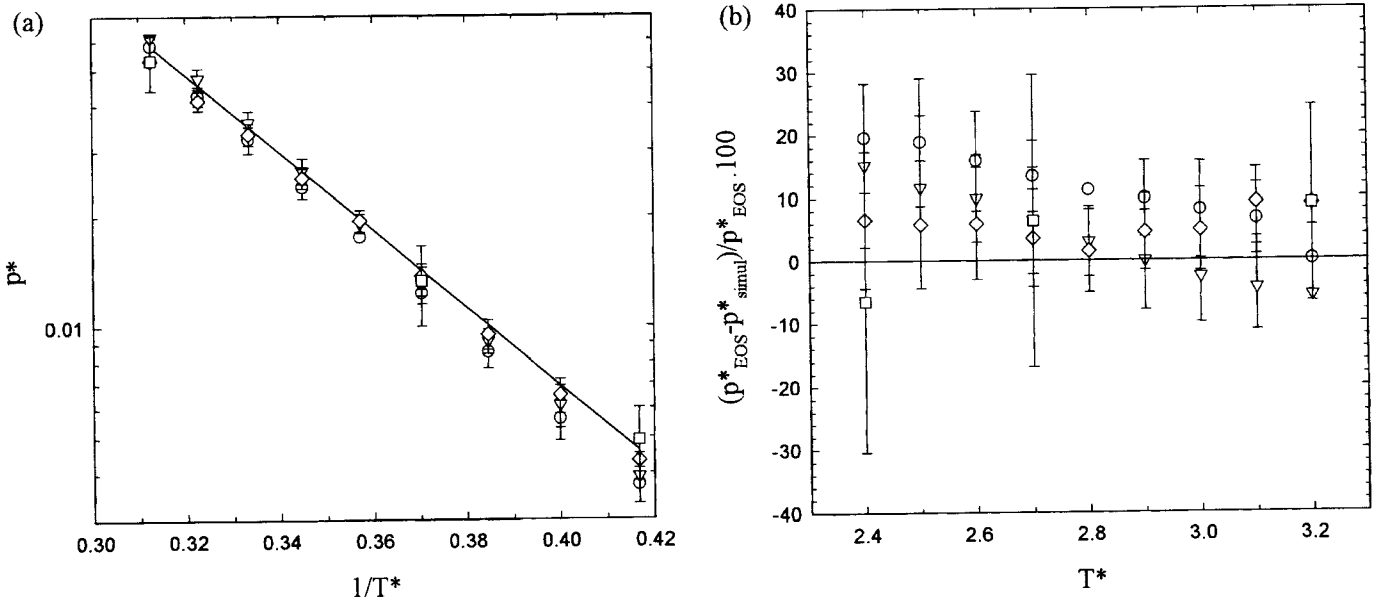

FIGURE 3 (a) Vapour pressure and (b) its relative deviations for 2CLJD fluid with $L = 0.505$ and $\mu^{*2} = 12$. (—, EOS; ○, GDI1; ∇, GDI2; ◇, GDI3; □, GEMC; see Tab. II for explanation of acronyms).

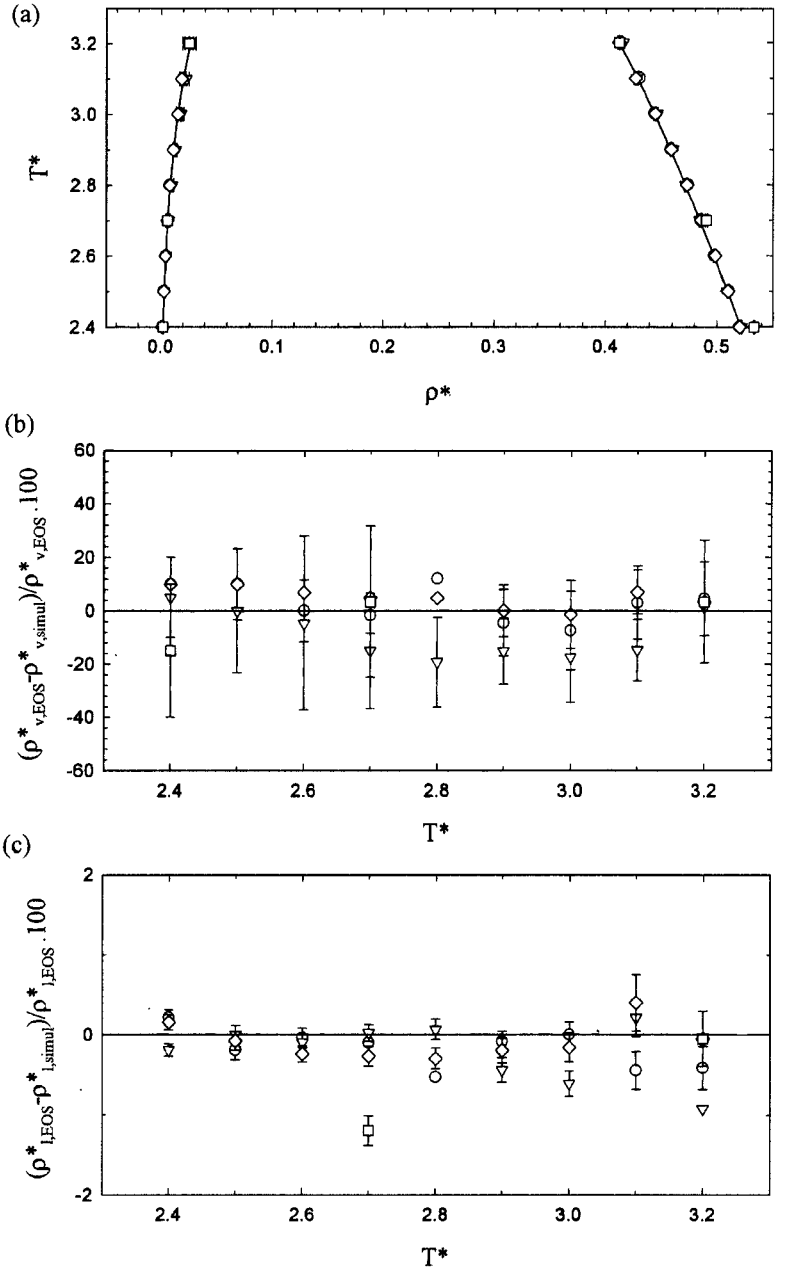

FIGURE 4 (a) Vapour–liquid coexistence envelope (b) relative deviations in saturated vapour density and (c) relative deviations in saturated liquid density for 2CLJD fluid with $L = 0.505$ and $\mu^{*2} = 12$. (—, EOS; ○, GDI1; ▽, GDI2; ◇, GDI3; □, GEMC; see Tab. II for explanation of acronyms).

TABLE III Vapour–liquid equilibrium data for the 2CLJD fluid with $L = 0.8$ and $\mu^{*2} = 9$ obtained from the physically based equation of state, Eq. (14), and direct simulations. The simulation uncertainties are given in the last digits as subscripts. EOS denotes data from the equation of state, GDI3 is the Gibbs-Duhem integration method starting from the Gibbs ensemble Monte Carlo coexistence point at $T^* = 2.2$ and using description of the vapour phase by the simple truncated virial equation of state, Eq. (11), at $T^* < 1.9$, and GEMC denotes the Gibbs ensemble Monte Carlo simulations. Vapour densities evaluated from the simple truncated virial equation of state, Eq. (11), at the vapour pressures are also added in parentheses

T^*	*EOS*	*GDI3*	*GEMC*
Vapour pressures			
1.5	0.00115	0.00079_{9}	
1.6	0.00236	0.00168_{60}	
1.7	0.00441	0.00328_{180}	
1.8	0.00762	0.00597_{270}	
1.9	0.01238	0.01035_{175}	0.01067_{82}
2.0	0.01909	0.01632_{233}	
2.1	0.02818	0.02460_{173}	
2.2	0.04015	0.03562	0.03562_{174}
2.3	0.05557	0.05013_{189}	
2.4	0.07516	0.06698_{173}	0.06608_{278}
Saturated liquid densities			
1.5	0.4345	0.4402_{39}	
1.6	0.4203	0.4265_{33}	
1.7	0.4054	0.4136_{47}	
1.8	0.3898	0.3984_{48}	
1.9	0.3732	0.3833_{57}	0.3882_{33}
2.0	0.3553	0.3641_{63}	
2.1	0.3357	0.3475_{110}	
2.2	0.3135	0.3243	0.3243_{640}
2.3	0.2875	0.3017_{128}	
2.4	0.2548	0.2662_{199}	0.2707_{89}
Saturated vapour densities			
1.5	0.00079	0.00054	
	(0.00079)	(0.00054)	
1.6	0.00154	0.00110	
	(0.00157)	(0.00110)	
1.7	0.00279	0.00206	
	(0.00285)	(0.00206)	
1.8	0.00471	0.00367	
	(0.00487)	(0.00368)	
1.9	0.00756	0.00623_{128}	0.00563_{57}
	(0.00798)	(0.00638)	(0.00662)
2.0	0.01169	0.01077_{212}	
	(0.01281)	(0.01025)	
2.1	0.01762	0.01535_{212}	
	(0.02139)	(0.01640)	
2.2	0.02623	0.02492	0.02492_{34}
		(0.03047)	(0.03047)
2.3	0.03926	0.03093_{257}	
2.4	0.06110	0.04355_{381}	0.06474_{86}

TABLE IV Vapour–liquid equilibrium data for the 2CLJD fluid with $L = 0.8$ and $\mu^{*2} = 12$ obtained from the physically based equation of state, Eq. (14), and direct simulations. The simulation uncertainties are given in the last digits as subscripts. EOS denotes data from the equation of state, GDI3 is the Gibbs-Duhem integration method starting from the Gibbs ensemble Monte Carlo coexistence point at $T^* = 2.4$ and using description of the vapour phase by the simple truncated virial equation of state, Eq. (11), at $T^* < 2.0$, and GEMC denotes the Gibbs ensemble Monte Carlo simulations. Vapour densities evaluated from the simple truncated virial equation of state, Eq. (11), at the vapour pressures are also added in parentheses

T^*	*EOS*	*GDI3*	*GEMC*
Vapour pressures			
1.6	0.00077	0.00043_{35}	
1.7	0.00158	0.00092_{66}	
1.8	0.00295	0.00182_{11}	
1.9	0.00514	0.00335_{20}	
2.0	0.00841	0.00594_{106}	0.00705_{102}
2.1	0.01308	0.00980_{117}	
2.2	0.01951	0.01547_{155}	
2.3	0.02810	0.02351_{192}	
2.4	0.03931	0.03411	0.03411_{185}
2.5	0.05375	0.04811_{195}	
2.6	0.07251	0.05622_{216}	0.05716_{278}
2.7		0.08677_{176}	
Saturated liquid densities			
1.6	0.4389	0.4443_{35}	
1.7	0.4256	0.4340_{39}	
1.8	0.4119	0.4204_{42}	
1.9	0.3976	0.4078_{49}	
2.0	0.3827	0.3961_{54}	0.3963_{48}
2.1	0.3670	0.3781_{63}	
2.2	0.3502	0.3627_{76}	
2.3	0.3319	0.3470_{74}	
2.4	0.3117	0.3266	0.3266_{66}
2.5	0.2884	0.3030_{129}	
2.6	0.2598	0.2815_{130}	0.2753_{95}
2.7		0.2493_{260}	
Saturated vapour densities			
1.6	0.00049	0.00028	
	(0.00050)	(0.00028)	
1.7	0.00097	0.00056	
	(0.00099)	(0.00056)	
1.8	0.00175	0.00107	
	(0.00181)	(0.00107)	
1.9	0.00297	0.00191	
	(0.00312)	(0.00192)	
2.0	0.00478	0.00410_{85}	0.00429_{75}
	(0.00514)	(0.00337)	(0.00413)
2.1	0.00741	0.00672_{94}	
	(0.00831)	(0.00562)	
2.2	0.01118	0.01059_{135}	
	(0.01388)	(0.00926)	
2.3	0.01655	0.01601_{209}	
		(0.01614)	
2.4	0.02442	0.02449	0.02449_{36}
2.5	0.03672	0.03143_{45}	
2.6	0.05947	0.04256_{59}	0.05654_{73}
2.7		0.07230_{2805}	

TABLE V Vapour–liquid equilibrium data for the 2CLJD fluid with $L = 1.0$ and $\mu^{*2} = 9$ obtained from the physically based equation of state, Eq. (14), and direct simulations. The simulation uncertainties are given in the last digits as subscripts. EOS denotes data from the equation of state, GDI3 is the Gibbs-Duhem integration method starting from the Gibbs ensemble Monte Carlo coexistence point at $T^* = 1.9$ and using description of the vapour phase by the simple truncated virial equation of state, Eq. (11), at $T^* < 1.6$, and GEMC denotes the Gibbs ensemble Monte Carlo simulations. Vapour densities evaluated from the simple truncated virial equation of state, Eq. (11), at the vapour pressures are also added in parentheses

T^*	*EOS*	*GDI3*	*GEMC*
Vapour pressures			
1.2	0.00086	0.00014_2	
1.3	0.00208	0.00041_9	
1.4	0.00425	0.00105_{27}	
1.5	0.00770	0.00235_{49}	
1.6	0.01273	0.00487_{101}	0.00579_{75}
1.7	0.01965	0.00900_{49}	
1.8	0.02878	0.01526_{179}	
1.9	0.04047	0.02412	0.02412_{169}
2.0		0.03658_{218}	
2.1		0.05270_{139}	0.04914_{210}
2.2		0.07365_{156}	
Saturated liquid densities			
1.2	0.3184	0.4192_{36}	
1.3	0.2916	0.4075_{30}	
1.4	0.2638	0.3934_{40}	
1.5	0.2370	0.3768_{45}	
1.6	0.2126	0.3637_{42}	0.3610_{34}
1.7	0.1900	0.3436_{67}	
1.8	0.1670	0.3268_{77}	
1.9	0.1400	0.2999	0.2999_{57}
2.0		0.2854_{109}	
2.1		0.2546_{137}	0.2404_{92}
2.2		0.2182_{243}	
Saturated vapour densities			
1.2	0.00075	0.00011	
	(0.00077)	(0.00012)	
1.3	0.00171	0.00032	
	(0.00181)	(0.00032)	
1.4	0.00340	0.00078	
	(0.00368)	(0.00078)	
1.5	0.00607	0.00166	
	(0.00696)	(0.00167)	
1.6	0.01011	0.00380_{101}	0.00426_{65}
	(0.01371)	(0.00340)	(0.00414)
1.7	0.01611	0.00622_{58}	
		(0.00631)	
1.8	0.02521	0.01079_{177}	
		(0.01116)	
1.9	0.04055	0.01908	0.01908_{202}
		(0.02036)	(0.02036)
2.0		0.02525_{221}	
2.1		0.03967_{330}	0.0556_{721}
2.2		0.07182_{1245}	

TABLE VI Vapour–liquid equilibrium data for the 2CLJD fluid with $L = 1.0$ and $\mu^{*2} = 12$ obtained from the physically based equation of state, Eq. (14), and direct simulations. The simulation uncertainties are given in the last digits as subscripts. EOS denotes data from the equation of state, GDI3 is the Gibbs-Duhem integration method starting from the Gibbs ensemble Monte Carlo coexistence point at $T^* = 2.0$ and using description of the vapour phase by the simple truncated virial equation of state, Eq. (11), at $T^* < 1.7$, and GEMC denotes the Gibbs ensemble Monte Carlo simulations. Vapour densities evaluated from the simple truncated virial equation of state, Eq. (11), at the vapour pressures are also added in parentheses

T^*	*EOS*	*GDI3*	*GEMC*
Vapour pressures			
1.4	0.00168	0.00024_2	
1.5	0.00340	0.00060_4	
1.6	0.00614	0.00136_{13}	
1.7	0.01019	0.00284_{51}	0.00372_{65}
1.8	0.01580	0.00535_{46}	
1.9	0.02322	0.00960_{161}	
2.0	0.03271	0.01622	0.01622_{153}
2.1		0.02609_{209}	
2.2		0.04065_{184}	0.04364_{278}
Saturated liquid densities			
1.4	0.2948	0.4119_{42}	
1.5	0.2717	0.3992_{45}	
1.6	0.2482	0.3862_{50}	
1.7	0.2243	0.3724_{52}	0.3713_{38}
1.8	0.2000	0.3604_{51}	
1.9	0.1739	0.3437_{65}	
2.0	0.1430	0.3152	0.3152_{52}
2.1		0.3036_{107}	
2.2		0.2818_{126}	0.2677_{67}
Saturated vapour densities			
1.4	0.00129	0.00017	
	(0.00145)	(0.00018)	
1.5	0.00254	0.00041	
	(0.00305)	(0.00041)	
1.6	0.00455	0.00090	
	(0.00651)	(0.00090)	
1.7	0.00761	0.00207_{42}	0.00265_{53}
		(0.00184)	(0.00250)
1.8	0.01218	0.00417_{38}	
		(0.00345)	
1.9	0.01910	0.00732_{161}	
		(0.00641)	
2.0	0.03049	0.01241	0.01241_{177}
		(0.01236)	(0.01236)
2.1		0.01983_{370}	
2.2		0.03351_{566}	0.03183_{281}

examined for $L = 0.505$ and $\mu^{*2} = 9$ in the temperature range from $T^* = 2.45$ to 3.1 is generally good to very good. This temperature interval roughly corresponds to reduced temperatures T^*/T_C^* ranging from ~ 0.72 to

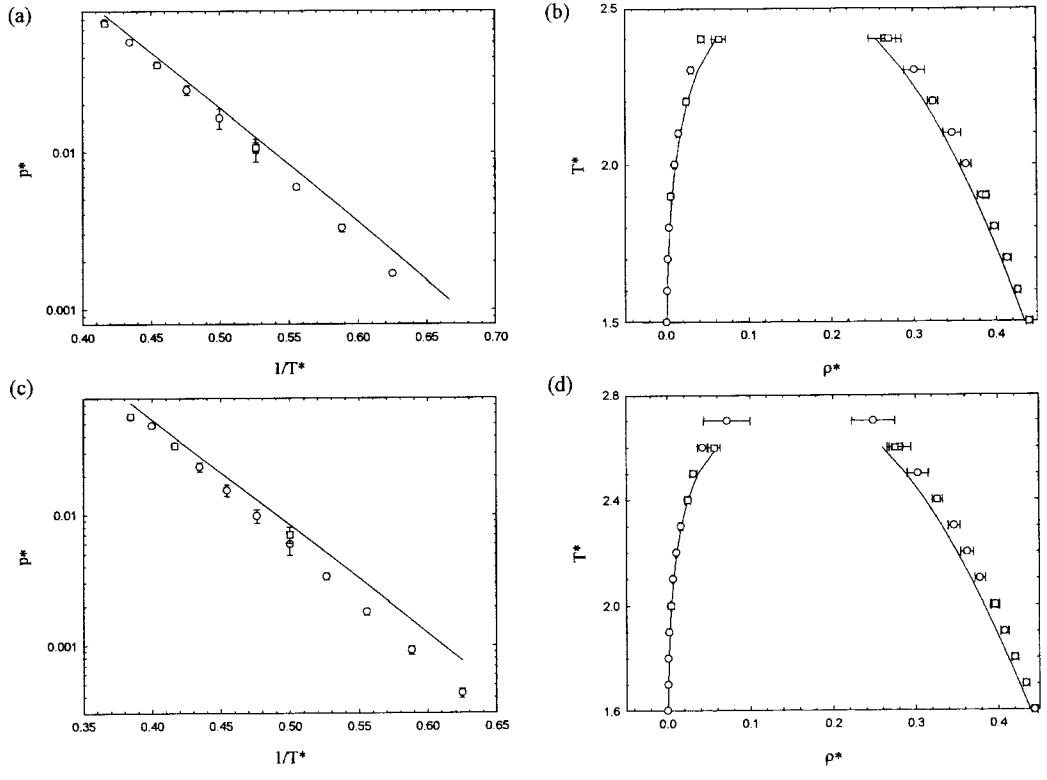

FIGURE 5 Vapour pressure and vapour–liquid coexistence curves for 2CLJD fluid with $L = 0.8$ and $\mu^{*2} = 9$ (*a*, *b*) and $\mu^{*2} = 12$ (*c*, *d*). (—, EOS; ○, GDI3; □, GEMC; see Tabs. III and IV for explanation of acronyms).

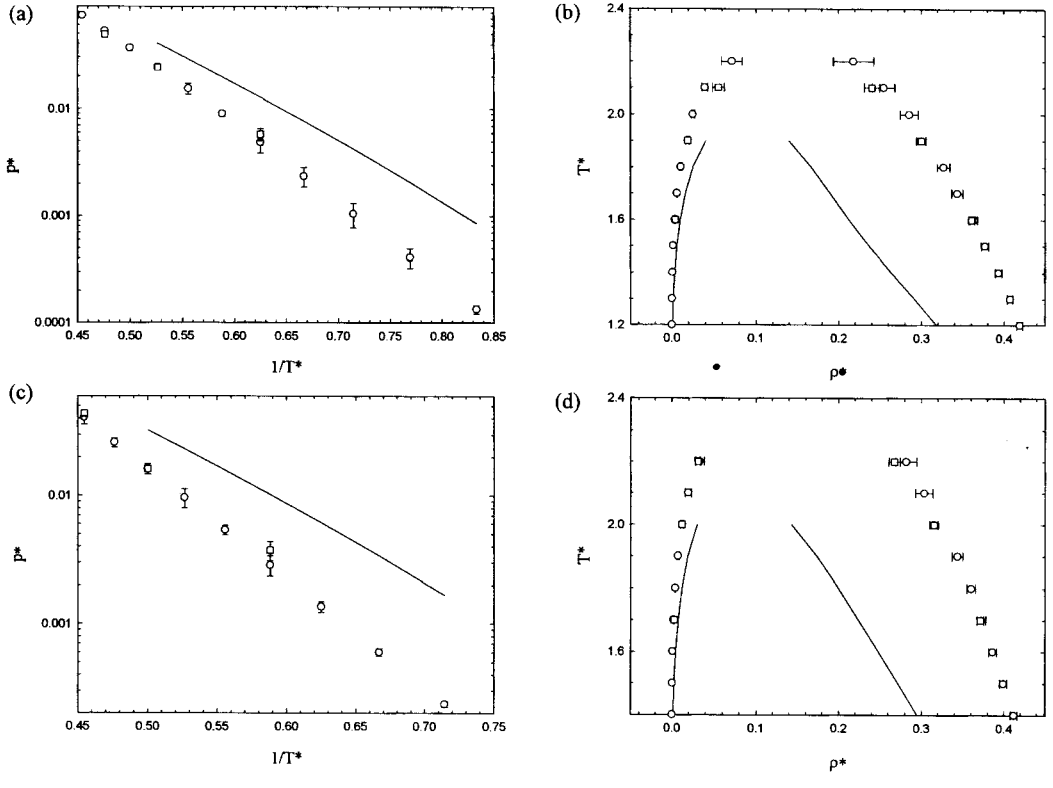

FIGURE 6 Vapour pressure and vapour–liquid coexistence curves for 2CLJD fluid with $L = 1.0$ and $\mu^{*2} = 9$ (*a*, *b*) and $\mu^{*2} = 12$ (*c*, *d*). (—, EOS; ○, GDI3; □, GEMC; see Tabs. V and VI for explanation of acronyms).

~ 0.92. (The critical temperature $T_C^* \approx 3.38$ was estimated by the critical scaling relation using the GDI3 simulation data and the result agrees well with $T_C^* = 3.405$ given by the physically based EOS [4].)

Regarding the vapour pressures, in most cases all methods mutually agree within the estimated statistical uncertainties. However, the percentagewise deviations (reaching up to 10%) exceed the limits of acceptance for engineering applications. There are no distinct differences between the different versions of the GDI runs used. From the nature of the differential equations involved it follows that the proper direction of integration is going from high temperatures downwards. In accordance with this, it is seen that the deviations between the GDI2 and GDI3 results do not propagate increasingly when the GDI run starts from slightly different state points at a high temperature while the GDI1 results (after starting from a moderate temperature) go slightly off at high temperature.

The mutual agreement in simulation results on saturated liquid densities is very good and within estimated statistical uncertainties in the data. The percentagewise errors are small enough so as to allow direct use of the computed densities in engineering applications.

In the first place, the results on saturated vapour densities document that the use of the simple truncated virial EOS is justified over a wide range of low temperatures. In most cases the data mutually agree within their estimated statistical uncertainties, but the percentagewise deviations are scattered, reach over 10% (and up to 20% at the lowest densities).

From the results for elongation $L = 0.505$ and $\mu^{*2} = 12$ obtained over the temperature range from $T^* = 2.4$ to 3.2 (see Tab. II and Figs. 3 and 4), analogous conclusions to the above can be drawn except that the GDI3 worked slightly better than the GDI1 and GDI2. The covered temperature range in this case corresponds to reduced temperatures T^*/T_C^* ranging from ~ 0.64 to ~ 0.86. (The critical temperature $T_C^* \approx 3.74$ was again estimated by the critical scaling relation using the GDI3 simulation data and the result agrees with $T_C^* = 3.745$ given by the physically based EOS [4].)

The comparisons of the VLE data calculated from the physically based EOS with the simulation results over the examined ranges of conditions for $L = 0.505$ show that the EOS represents a reasonable compromise between all the simulation data obtained. Not surprisingly, the GEMC works well for the VLE over a wide range of moderate conditions, *i.e.*, except for the vicinity of the critical point (which region represents a general problem of the simulation methods) and the region of low temperatures, where the GDI should apparently be preffered.

5.2. Performance of Physically Based Equation of State for Large Elongations and Dipole Moments

For the 2CLJD fluid with $L = 0.8$, and $\mu^{*2} = 9$ and 12 (see Tabs. III and IV, and Fig. 5), the overall agreement between simulated VLE data and results from the physically based EOS is relatively fair. The vapour pressures resulting from the EOS are typically by about 10% higher than those obtained from simulations whereas the simulated orthobaric densities are typically by about 5% higher than those from the EOS.

Nevertheless, it is seen that the performance of the EOS further rapidly deteriorates with increasing elongation L. Tables V and VI as well as Figure 6 then clearly show that the EOS completely fails to reproduce the simulated VLE data for the elongation $L = 1.0$. This means that the EOS cannot be used to extrapolate to elongations approaching this value.

An interesting finding is that the deviations between simulation data and the EOS results do not seem to be substantially affected by the size of the dipole moment. Furthermore, as it has been shown by Müller *et al.* [12], the dependence of the dipolar term of the EOS on the elongation is rather weak. These facts indicate that the inadequacy of the physically based EOS at high elongations is rather due to the failure of the attraction term of the EOS, which was fitted to simulation data base wherein the uppermost elongation value was 0.67. Particularly in view of this underlying limitation, the extrapolation power of the physically based EOS for elongations up to $L = 0.8$ at values of μ^{*2} up to 12 may be considered still reasonable.

6. CONCLUSIONS

Generally, good mutual agreement within statistical uncertainties of the simulation methods employed in the present study on 2CLJD fluid, *i.e.*, the Gibbs ensemble Monte Carlo, the variants of the Gibbs-Duhem integration combined with NPT molecular dynamics, and the NpT plus test particle method is observed in the calculated vapour pressures and saturated vapour and liquid densities along the entire vapour–liquid coexistence locus of the 2CLJD fluid. An effective combination of the GEMC and GDI methods may be recommended to cover rapidly the VLE coexistence dome over a widest possible range of conditions. However, the size of statistical uncertainties in the vapour pressures should be kept in mind in engineering applications.

The physically based equation of state for the 2CLJD fluid in the present form represents a good compromise between the results from different examined simulation methods up to moderate elongations. In the parametric region of large elongations and high dipole moments, the results obtained for VLE from the physically based EOS deteriorate rapidly with increasing elongation. This shortcoming may be ascribed to the attraction term of the EOS which was fitted to simulation data only up to elongation of $L = 0.67$.

The obtained accurate simulation data supplement the existing base of thermodynamic data for the model 2CLJD fluid and extend their coverage to the region of molecular parameters still relevant and important for the calculation of thermodynamic properties of real fluid systems. The extended database makes it possible to continue the work on developing and improving the analytical equation of state, particularly addressing the problem of describing the systems constituted of molecules with high elongation.

Acknowledgements

Fruitful discussions with Matthias Mecke from the University Halle-Wittenberg are gratefully acknowledged. The research was supported by the Grant Agency of the Academy of Sciences of the Czech Republic (Grant No. A-4072712) and by the program KONTAKT for cooperation between the Czech Republic and Austria.

APPENDIX

The Physically Based Equation of State for the 2CLJD Fluid

The 2CLJD-EOS [4] is written as

$$F_{2\mathrm{CLJD}}(T^*, \rho^*, L, \mu^{*2}) = F_H(T^*, \rho^*, L) + F_A(T^*, \rho^*, L) + F_D(T^*, \rho^*, \mu^{*2}) \tag{14}$$

The hard body term F_H is taken from Boublík and Nezbeda [5] as

$$\frac{F_H}{N\mathrm{k_B}T} = (\alpha^2 - 1)\ln(1 - \eta) + \frac{(\alpha^2 + 3\alpha)\eta - 3\alpha\eta^2}{(1 - \eta)^2} \tag{15}$$

where the anisotropy parameter α is a function of L, $\alpha = \alpha(L)$, and the packing fraction η depends linearly on ρ^*, $\eta = \rho^* C(L,T^*)$. The functional relations $\alpha = \alpha(L)$ and $C = C(L,T^*)$ are given by Mecke *et al.* [3].

The attractive term F_A was derived by Mecke *et al.* [3] and writes as

$$\frac{F_A}{N k_B T} = \sum_i^{34} c_i \left(\frac{T^*}{T_p^*}\right)^{m_i} \left(\frac{\rho^*}{\rho_p^*}\right)^{n_i} \alpha^{o_i} \exp\left[p_i \left(\frac{\rho^*}{\rho_p^*}\right)^{q_i}\right] \tag{16}$$

The so-called pseudocritical temperature T_p^* and the pseudocritical density ρ_p^* are also functions of L. The functional relations $T_p^* = T_p^*(L)$ and $\rho_p^* = \rho_p^*(L)$, the coefficients c_i as well as the exponents m_i, n_i, o_i, p_i and q_i are also taken as given by Mecke *et al.* [3].

The dipolar contribution F_D was derived by Saager and Fischer [2] on the basis of extensive simulations for $L = 0.505$ and is given as

$$\frac{F_D}{N k_B T} = \sum_i^{28} \bar{c}_i \left(\frac{T^*}{T_p^*}\right)^{\bar{n}_i/2} \left(\frac{\rho^*}{\rho_p^*}\right)^{\bar{m}_i/2} (\mu^{*2})^{\bar{k}_i/4} \exp\left[-\bar{o}_i \left(\frac{\rho^*}{\rho_p^*}\right)^2\right] \tag{17}$$

The coefficients $\bar{c}_i$ as well as the exponents $\bar{n}_i, \bar{m}_i, \bar{k}_i$ and $\bar{o}_i$ are given by Saager and Fischer [2] or by Kriebel *et al.* [10, 11].

References

[1] Saager, B., Hennenberg, R. and Fischer, J. (1992). Construction and application of physically based equations of state. Part I. Modification of the BACK equation, *Fluid Phase Equilib.*, **72**, 41–66.

[2] Saager, B. and Fischer, J. (1992). Construction and application of physically based equations of state. Part II. The dipolar and quadrupolar contributions to the Helmholtz energy, *Fluid Phase Equilib.*, **72**, 67–88.

[3] Mecke, M., Müller, A., Winkelmann, J. and Fischer, J. (1997). An equation of state for two-center Lennard-Jones fluids, *Int. J. Thermophys.*, **18**, 683–698; Erratum, *Int. J. Thermophys.*, **19**, (1998), 1495.

[4] Kriebel, Ch., Mecke, M., Winkelmann, J., Vrabec, J. and Fischer, J. (1998). An equation of state for dipolar two-center Lennard-Jones molecules and its application to refrigerants, *Fluid Phase Equilib.*, **142**, 15–32.

[5] Boublík, T. and Nezbeda, I. (1986). P–v–T behaviour of hard body fluids: theory and experiment, *Collect. Czech. Chem. Commun.*, **51**, 2301–2432.

[6] Smith, W. R., In: Singer, K. (Ed.), *Specialist Periodical Reports, Statistical Mechanics*, **1**, Chemical Society, London, 1973, 71.

[7] Mecke, M., Müller, A., Winkelmann, J., Vrabec, J., Fischer, J., Span, R. and Wagner, W. (1996). An accurate van der Waals-type equation of state for Lennard-Jones fluid, *Int. J. Thermophys.*, **17**, 391–404.

[8] Lísal, M. and Vacek, V. (1996). Direct evaluation of vapour–liquid equilibria by molecular dynamics using Gibbs-Duhem integration, *Mol. Sim.*, **17**, 27–39.

[9] Saager, B., Fischer, J. and Neumann, M. (1991). Reaction field simulations of monoatomic and diatomic fluids, *Mol. Sim.*, **6**, 27–49.

[10] Kriebel, Ch., Müller, A., Winkelmann, J. and Fischer, J. (1996). A hybrid equation of state for Stockmayer pure fluids and mixtures, *Fluid Phase Equilib.*, **119**, 67–80.

[11] Kriebel, Ch. and Winkelmann, J. (1997). Vapour–liquid equilibria for Stockmayer fluids with rigid and polarizable dipoles, *Mol. Phys.*, **90**, 297–301.
[12] Müller, A., Winkelmann, J. and Fischer, J. (1993). Effect of molecular elongation on the dipolar free energy, *J. Chem. Phys.*, **99**, 3946–3949.
[13] Kriebel, Ch., Müller, A., Winkelmann, J. and Fischer, J. (1996). Prediction of thermodynamic properties for fluid nitrogen with molecular dynamics simulations, *Int. J. Thermophys.*, **17**, 1349–1363.
[14] Müller, A., Winkelmann, J. and Fischer, J. (1996). Backone family of equation of state: 1. Nonpolar and polar pure fluids, *AIChE J.*, **42**, 1116–1126.
[15] Calero, S., Wendland, M. and Fischer, J. (1998). Description of alternative refrigerants with BACKONE equations, *Fluid Phase Equilib.*, **152**, 1–22.
[16] Müller, A., Heene-Medina, D., Wendland, M., Vrabec, J., Winkelmann, J. and Fischer, J., Specific mixing rules: Test and application, *13th Symposium on Thermophysical Properties*, Boulder, Colorado USA, p. 226.
[17] Lísal, M., Budinský, R. and Vacek, V. (1997). Vapour–liquid equilibria for dipolar two-centre Lennard-Jones fluids by Gibbs-Duhem integration, *Fluid Phase Equilib.*, **135**, 193–207.
[18] Lísal, M., Budinský, R., Vacek, V. and Aim, K. (1999). Vapour–liquid equilibria of alternative refrigerants by molecular dynamics simulations, *Int. J. of Thermophys.*, **20**, 163–174.
[19] Lotfi, A., Vrabec, J. and Fischer, J. (1992). Vapour–liquid equilibria of the Lennard-Jones fluid from the NpT plus test particle, *Mol. Phys.*, **76**, 1319–1333.
[20] Kofke, D. A. (1993). Direct evaluation of phase coexistence by molecular simulation *via* integration along the saturation line, *J. Chem. Phys.*, **98**, 4149–4162.
[21] Panagiotopoulos, A. Z. (1992). Direct determination of fluid phase equilibria by simulation in the Gibbs ensemble: A review, *Mol. Sim.*, **9**, 1–23.
[22] Allen, M. P. and Tildesley, D. J., *Computer Simulation of Liquids*, Clarendon Press, Oxford, 1987.
[23] Stroud, A. H., *Approximate Calculation of Multiple Integrals*, Prentice Hall, 1971.
[24] Goodwin, A. R. H. and Moldover, M. R. (1990). Thermophysical properties of gaseous refrigerants from speed of sound measurements. I. Apparatus, model, and results for 1,1,1,2-tetrafluoroethane R134a, *J. Chem. Phys.*, **93**, 2741–2753.
[25] Gupta, S., Yang, J. and Kestner, N. R. (1988). Computer modelling of liquid propane using three-site potential models, *J. Chem. Phys.*, **89**, 3733–3741.
[26] Guissani, Y. and Guillot, B. (1993). A computer simulation study of the liquid–vapour coexistence curve of water, *J. Chem. Phys.*, **98**, 8221–8235.
[27] Vrabec, J., Vorhersage thermodynamischer Stoffdaten durch molekulare Simulation, VDI-Fortschritt-Berichte, VDI-Verlag Düsseldorf, 1996.
[28] Nezbeda, I. and Kolafa, J. (1995). The use of control quantities in computer simulation experiments: Application to the Exp-6 potential fluid, *Mol. Sim.*, **15**, 153–163.